Preparation and electrochemical performances of nanoporous/cracked cobalt oxide layer for supercapacitors

Fereydoon Gobal · Masoud Faraji

Abstract Nanoporous/cracked structures of cobalt oxide (Co_3O_4) electrodes were successfully fabricated by electroplating of zinc–cobalt onto previously formed TiO_2 nanotubes by anodizing of titanium, leaching of zinc in a concentrated alkaline solution and followed by drying and annealing at 400 °C. The structure and morphology of the obtained Co_3O_4 electrodes were characterized by X-ray diffraction, EDX analysis and scanning electron microscopy. The results showed that the obtained Co_3O_4 electrodes were composed of the nanoporous/cracked structures with an average pore size of about 100 nm. The electrochemical capacitive behaviors of the nanoporous Co_3O_4 electrodes were investigated by cyclic voltammetry, galvanostatic charge–discharge studies and electrochemical impedance spectroscopy in 1 M NaOH solution. The electrochemical data demonstrated that the electrodes display good capacitive behavior with a specific capacitance of 430 F g^{-1} at a current density of 1.0 A g^{-1} and specific capacitance retention of ca. 80 % after 10 days of being used in electrochemical experiments, indicating to be promising electroactive materials for supercapacitors. Furthermore, in comparison with electrodes prepared by simple cathodic deposition of cobalt onto TiO_2 nanotubes (without dealloying procedure), the impedance studies showed improved performances likely due to nanoporous/cracked structures of electrodes fabricated by dealloying of zinc, which provide fast ion and electron transfer routes and large reaction surface area with the ensued fast reaction kinetics.

F. Gobal · M. Faraji (✉)
Department of Chemistry, Sharif University of Technology,
P.O. Box 11365-9516, Tehran, Iran
e-mail: masoudfaraji@mehr.sharif.ir

1 Introduction

Electrochemical capacitors (ECs) or supercapacitors are commonly used as an electrochemical energy storage device, which is ideally suitable for rapid storage and release of energy. Electrochemical capacitors are divided into two categories according to different energy storage mechanisms as electrochemical double-layer capacitors (EDLCs) and electrochemical pseudocapacitors (EPCs). The capacitance of EDLCs is based on charge separation at the electrode/electrolyte interface, while the capacitance of EPCs arises from fast and reversible faradic redox reactions of the electroactive materials [1, 2]. RuO_2 has been recognized as one of the most promising electrode materials due to its high specific capacitance, but it is too expensive to be widely used in practice. Hence, considerable efforts have been devoted to develop alternative electrode materials such as iron oxide (Fe_3O_4), vanadium oxide (V_2O_5), cobalt oxide (Co_3O_4) and manganese dioxide (MnO_2) [3]. Cobalt oxide, because of its favorable capacitive characteristics and environmental friendliness, is generally considered as promising electrode materials for EPCs. It is remarkable that the theoretical specific capacitance of Co_3O_4 is estimated around 3,560 F g^{-1} [4]. Pseudocapacitance of Co_3O_4 originates from fast and reversible surface or near-surface phenomena involved during the faradaic reactions. To improve the supercapacitor performance, it is crucial to enhance the kinetics of ion and electron transport inside the electrodes and at the electrode/electrolyte interface. An effective way is to fabricate films with nanoporous structures which provide relatively short diffusion pathway for ions as well as large active surface leading to high charge capacities and high utilization of active materials [5, 6]. The mesoporous texture of substrate can significantly affect microstructures of

Co_3O_4 leading to high charge capacities and short diffusion paths for ion transport which may improve the performance of electrochemical supercapacitors. Among various substrates, TiO_2 nanotubes fabricated by anodizing titanium can be used as an appropriate substrate for electrodeposition of Co_3O_4 because of its high surface area, thermal stability, controlled pore structure and relatively low cost [7]. TiO_2 nanotubes/Ti substrate contributes only a small electric double-layer capacitance of around 3 mF cm^{-2} at a constant current density of 10 μA cm^{-2} [8]. The distinct nanotubular structure seems to increase the dispersion of active materials and result in the enhancement of capacitance.

The synthesis of porous Co_3O_4 as supercapacitor has always been challenging. A large number of studies have focused on the fabrication of porous Co_3O_4 based on pulsed laser deposition and plasma spray technique [9, 10]. Most of these methods require complex apparatus and are sophisticated techniques. Therefore, it is desirable to explore simple methods to fabricate Co_3O_4 nanostructure for application in supercapacitors. In the present work, we report the synthesis of nanoporous Co_3O_4/TiO_2 nanotubes/Ti electrode using dealloying of Co–Zn/TiO_2 nanotubes/Ti structure in alkaline solution. To the best of our knowledge, this is the first report on the nanoporous Co_3O_4 fabricated by dealloying procedure as the electrode material for supercapacitors.

2 Experimental procedure

2.1 Preparation of the Co_3O_4/TiO_2 nanotubes/Ti electrode

Titanium dioxide nanotubes were grown on stripes of Ti (99 % purity) with a geometric area of 3 cm^2 according to [11]. Very briefly, Ti stripes were polished with emery papers no 400–3,000 to obtain a mirror finish and subsequently cleaned in acetone and deionized water in an ultrasonic bath. The cleaned samples were anodized at 30 V for 2 h in ethylene glycol containing 0.5 wt% ammonium fluoride and 2.5 wt% of water at room temperature in a two-electrode cell using platinum foil as a counter electrode. The anodized samples were further washed with deionized water and ultrasonically cleaned for 60 s in deionized water to remove surface debris and subsequently dried in air. The anodized samples were annealed at 450 °C for 2 h to form the anatase phase.

Co–Zn alloy was galvanostatically electroplated onto TiO_2 nanotubes/Ti electrodes at a current density of 10 mA cm^{-2}. Bath composition and electroplating conditions are given in Table 1. The electrodes were deposited

Table 1 The optimized bath composition and electroplating conditions

Bath composition	Co–Zn (g l^{-1})	Co alone (g l^{-1})	Electroplating conditions
$ZnCl_2$	5.00	0.00	$T = 25\ °C$
$CoCl_2 \cdot 6(H_2O)$	3.00	3.00	pH 5.5
H_3BO_3	3.50	3.50	Anode: Zn
			Current density: 10 mA cm^{-2}
KCl	21.00	21.00	Electroplating time: 20 min

for 20 min. After electroplating, the electrodes were treated in 2 M NaOH at room temperature for 48 h until no more hydrogen evolution was observed. Treatment in alkali dissolves a good portion of the electrodeposited zinc producing a porous cobalt layer of high surface area. A few potential cyclic in the range of −0.5 to 1 V versus Ag/AgCl was subsequently executed on the electrodes in 1.0 M NaOH solution to form a complete $Co(OH)_2/TiO_2$ nanotubes/Ti composite. Finally, heat treatment at 400 °C for 2 h was carried out to convert the as-prepared $Co(OH)_2/TiO_2$ nanotubes/Ti to crystalline Co_3O_4/TiO_2 nanotubes/Ti and keep the redox electroactivity of Co_3O_4 to the full degree. These electrodes are denoted as electrode A. The results of the chemical composition analysis reveal that after the dealloying treatment there is still a low percentage of zinc present in the coatings, which corresponds to the zinc occluded down to a metal layer [12]. Therefore, it is expected that a small amount of ZnO would remain in the deposited coatings after calcination. Also, electroplating of Co alone onto TiO_2 nanotubes/Ti electrodes for 20 min and then calcination were carried out at the same conditions to investigate the influence of dealloying of Zn on the morphology of Co_3O_4 deposit and its capacitance. These electrodes are denoted as electrode B.

2.2 Characterization and electrochemical studies

Morphological studies were carried out by a scanning electron microscope (Philips, Model XL30). Chemical compositions were determined by EDX in a scanning electron microscope (VEGA\\Tescan). The crystallographic structures of the materials were determined by X-ray diffraction (XRD). Capacitance measurements were performed by BHP + 6230 potentiostat/galvanostat. Cyclic voltammetry (CV) and electrochemical impedance studies were carried out using Voltalab10 electrochemical system. All electrochemical studies were performed in a conventional three-electrode cell where all potentials are reported against Ag/AgCl reference electrode at room temperature and 1.0 M NaOH was the electrolyte throughout the studies.

3 Results and discussion

3.1 Morphology characterization

The surface morphology and microstructure of the prepared electrodes are shown in Fig. 1. Figure 1a shows the scanning electron microscopy (SEM) image of bare TiO_2 nanotubes/Ti where distinct and well-resolved nanotubes are visible. The inner diameter of TiO_2 nanotubes/Ti is 40–80 nm and the wall thickness is 5–10 nm. Figure 1b shows the SEM image of the electrode B. As it can be seen in Fig. 1b, Co_3O_4 film has covered the entire surface of TiO_2 nanotubes/Ti and despite high surface area, porosity of this electrode is not very high. Porosity is crucial to enhance the active material–electrolyte interfacial area and faster ion transfer inside the pore structure in supercapacitor applications [13, 14]. Therefore, less contact between the electrode materials and the electrolyte leads to a decrease in the performance of this electrode. The surface SEM images of Co–Zn/TiO_2 nanotubes/Ti electrode (before dealloying of Zn) and electrode A (after dealloying and then calcination) are shown in Fig. 1c, d, respectively. As seen from Fig. 1d, the surface morphology of electrode A is very different and consists of nanoporous/cracks where cracks sizes are ranging from around 50–200 nm. These extra cracks and nanopores enhance the accessibility of the internal area to the electrolyte and promote the transport of reactive species into the electrode, thereby resulting in increase in the available electrochemically active sites which improve the performance of electrochemical supercapacitors.

The surface compositions of the deposits both before and after dealloying were analyzed by EDX where the results are presented in Fig. 2. The surface before dealloying contained 20.79 % Co and 69.33 % Zn (at.%) (Fig. 2a). After alkaline dealloying, the surface composition changed to 63.12 % Co and 6.98 % Zn (at.%) (Fig. 2b). Figure 3 shows XRD patterns of annealed TiO_2 nanotubes/Ti electrode and electrode A. The peaks with 2θ of 25.3° and 48.2° are assigned to anatase crystal structure
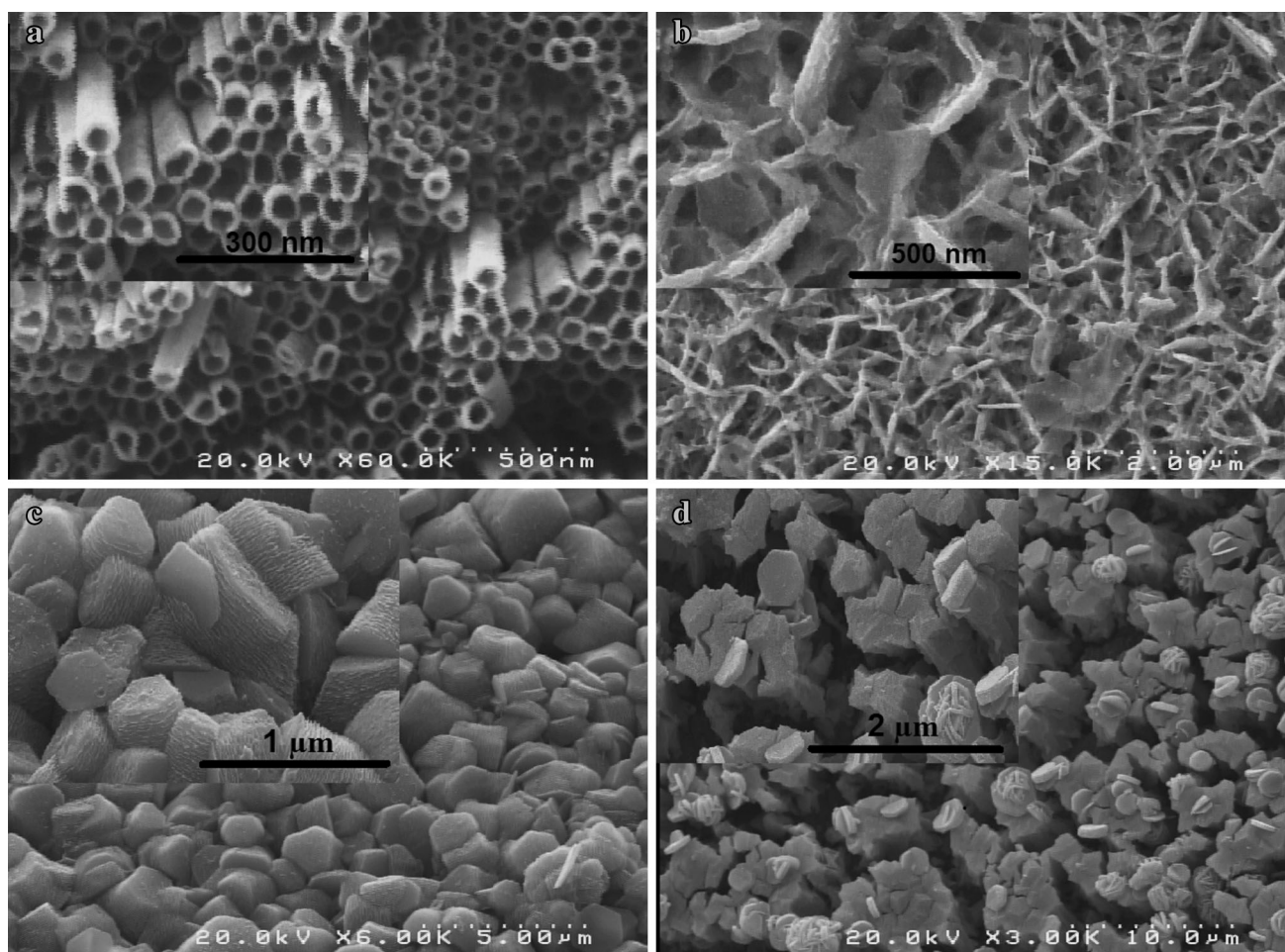
Fig. 1 SEM images of bare TiO_2 nanotubes/Ti electrode (**a**), electrode B (**b**), Co–Zn/TiO_2 nanotubes/Ti electrode (**c**) and electrode A (**d**)

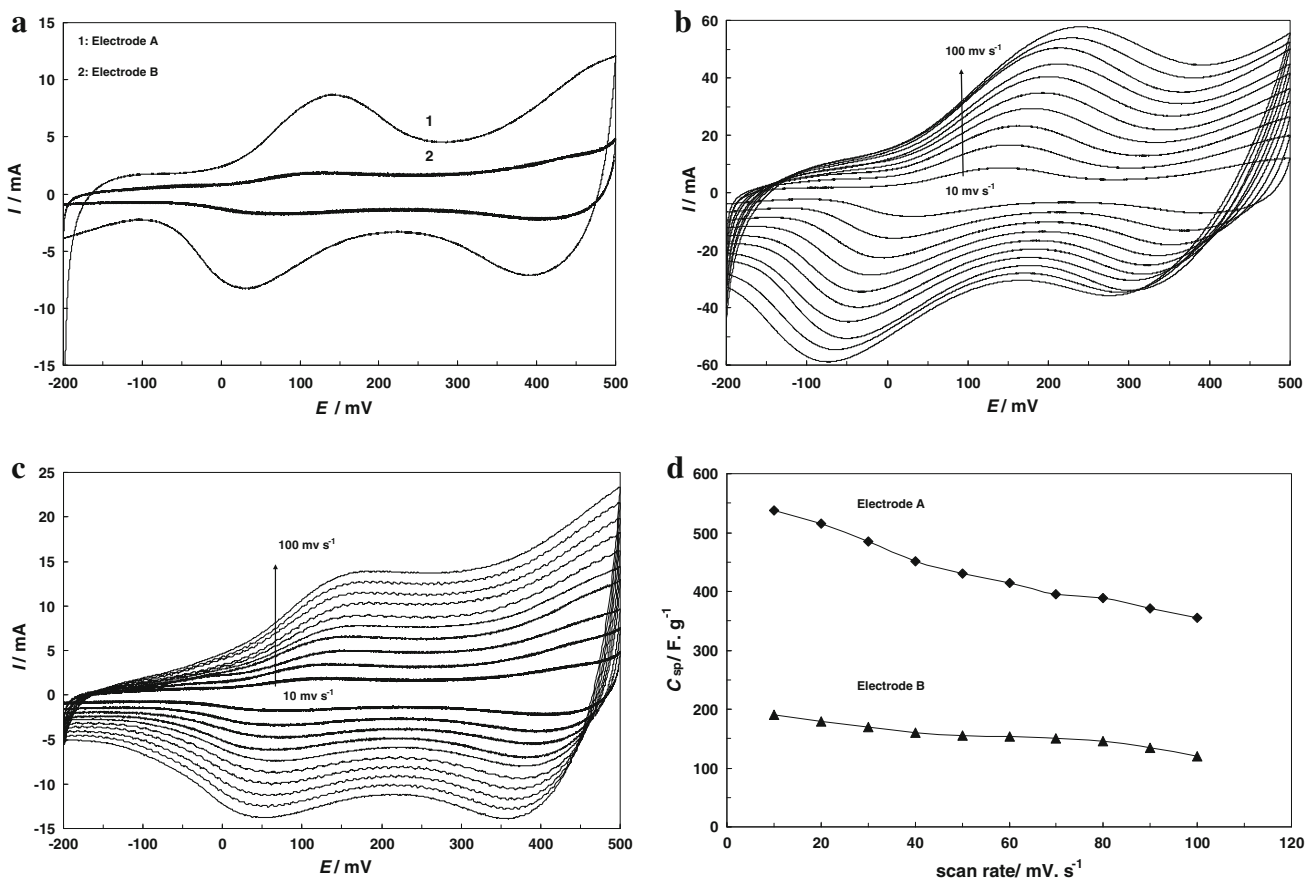**Fig. 2** EDX spectra obtained of Co–Zn/TiO$_2$ nanotubes/Ti electrode before (**a**) and after dealloying (**b**)
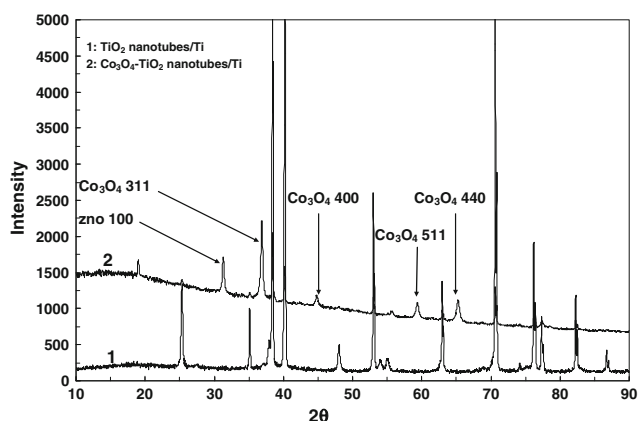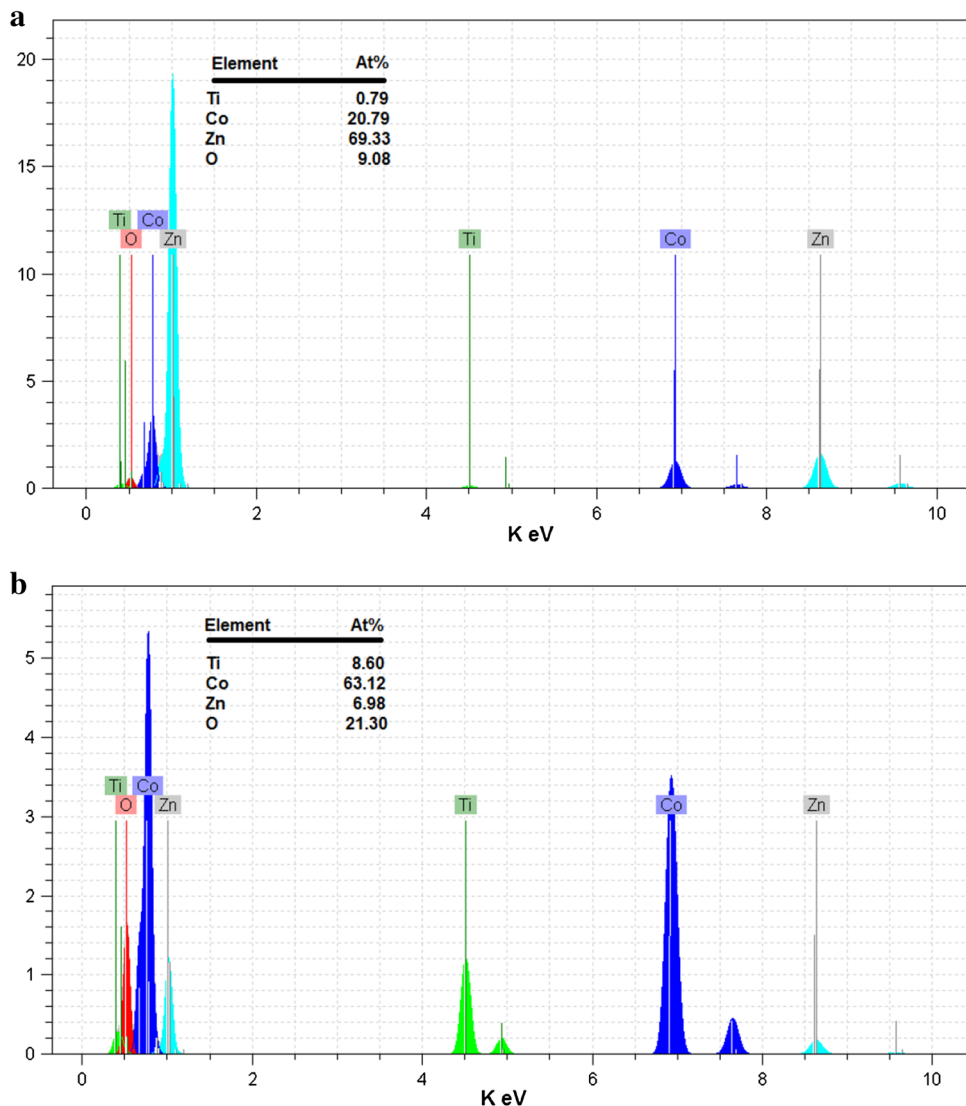
Fig. 3 XRD patterns of TiO$_2$ nanotubes/Ti electrode and electrode A

peaks. The diffraction peaks of Co$_3$O$_4$ at 36.85°, 44.81°, 59.36° and 65.24° can be assigned to as (3 1 1), (4 0 0), (5 1 1) and (4 4 0) reflections, respectively. Also, the diffraction peak at around 33° is attributed to crystalline ZnO. Zinc oxide results in the course of the calcination of our electrodes through the oxidation of the remaining un-leached Zn. According to our EDX results, Zn content is no more than 7 % of the electroactive material, and it is largely located in the bulk of the deposit, otherwise it would have been leached out.

3.2 Cyclic voltammograms

Cyclic voltammetry (CV) was employed to investigate the effect of dealloying of Zn on the capacitive behavior of the prepared electrodes. Figure 4a compares the cyclic voltammograms of electrodes A and B at the potential range of −0.2 to 0.5 V versus Ag/AgCl in 1.0 M NaOH electrolyte

of TiO$_2$NTs while lines at 40.4° and 38.5° correspond to crystalline Ti metal. After deposition of oxide films (electrode A), the samples XRD patterns exhibit new

Fig. 4 Cyclic voltammogram of the electrode A and B in 1.0 M NaOH solution at a scan rate of 10 mV s^{-1} (**a**), cyclic voltammograms obtained in 1.0 M NaOH for the electrode A (**b**) and electrode B (**c**) in various scan rates. The plot of variation of the specific capacitance of both electrodes (A and B) with scan rate (**d**)

with a scan rate of 10 mV s^{-1}. Although the CV shapes of the two electrodes are similar, the peak current for the electrode A is higher. This improvement is due to the higher surface area produced by extra cracks and nanopores of this electrode (see Fig. 1d) that enhances the accessibility of the interface to ions. As seen from Fig. 4a, a pair of well-defined broad redox peaks is visible in the CV patterns, indicating that the electrochemical capacitance of the Co$_3$O$_4$/TiO$_2$ nanotubes/Ti electrode mainly arises from the pseudocapacitance according to the following e-transfer processes [15]:

$$Co_3O_4 + OH^- + H_2O \rightleftarrows 3CoOOH + e^- \qquad (1)$$

$$CoOOH + OH^- \rightleftarrows CoO_2 + H_2O + e^- \qquad (2)$$
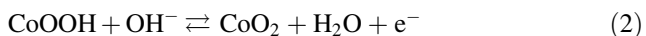
As mentioned before, ZnO is the by-product of dealloying and calcination and, thus, its existence is inevitable in the final electrode. Although it has been shown [16, 17] that ZnO exhibits small to moderate electrochemical capacity, its contribution in this study seems negligible on accounts of its low content as signified by EDX study, being mainly in the bulk of the material (otherwise, it would have been

leached out) and largely not in contact with the electrolyte. It thus can be concluded that the capacitive behavior of the electrode A (fabricated by dealloying procedure) is mostly, if not entirely, caused by the presence of Co$_3$O$_4$. However, small pseudocapacitance of ZnO in the alkaline solution which can have only a minor to negligible contribution cannot be entirely dismissed.

The voltammetric charge (*q*) integrated from a positive or negative sweep of CV plots can be used as an effective criterion for determining the pseudocapacitance in redox transitions [18, 19]. Using Eq. (3), the specific capacitance of 530 F g^{-1} is obtained at 10 mV s^{-1} potential sweep rate in 1.0 M NaOH for the electrode A, compared with 190 F g^{-1} for the electrode B.

$$C_{SP} = \frac{q}{mv} = \frac{1}{0.7mv} \int_{-0.2}^{0.5} i(V)dV \qquad (3)$$

In Eq. (3), *i*, *v* and *m* are indicative of the response current (mA), the potential scan rate (V s^{-1}) and the active material mass, respectively.

The effect of different scan rates on the capacitive behavior of the electrodes A and B has been studied, and results are presented in Fig. 4b, c. It is observed that the anodic peaks shift toward high potential and cathodic peaks shift negatively upon increasing the potential scan rate pointing to the quasi-reversible nature of the redox couples [20]. Also, the anodic and cathodic peak current densities for both electrodes are relatively similar, indicating that charge and the discharge occur reversibly at the electrode/ electrolyte interface.

A plot of the specific capacitance of both electrodes (A and B) at different scan rates is shown in Fig. 4d. The specific capacitance decreases from 530 to 350 F g^{-1} for the electrode A and 190 to 120 F g^{-1} for the electrode B as the scan rate is increased from 10 to 100 mV s^{-1}. The decrease in capacitance is attributed to the presence of inner active sites that do not undergo the redox transitions at higher scan rates. This is probably due to the slow diffusion of OH^{-} inside the porous electrode. The decreasing capacitance suggests that parts of the surface of the electrode are inaccessible at high charge/discharge rates. Hence, the specific capacitance obtained at the slowest scan rate is believed to be closest to that of full utilization of the electrode material [13].
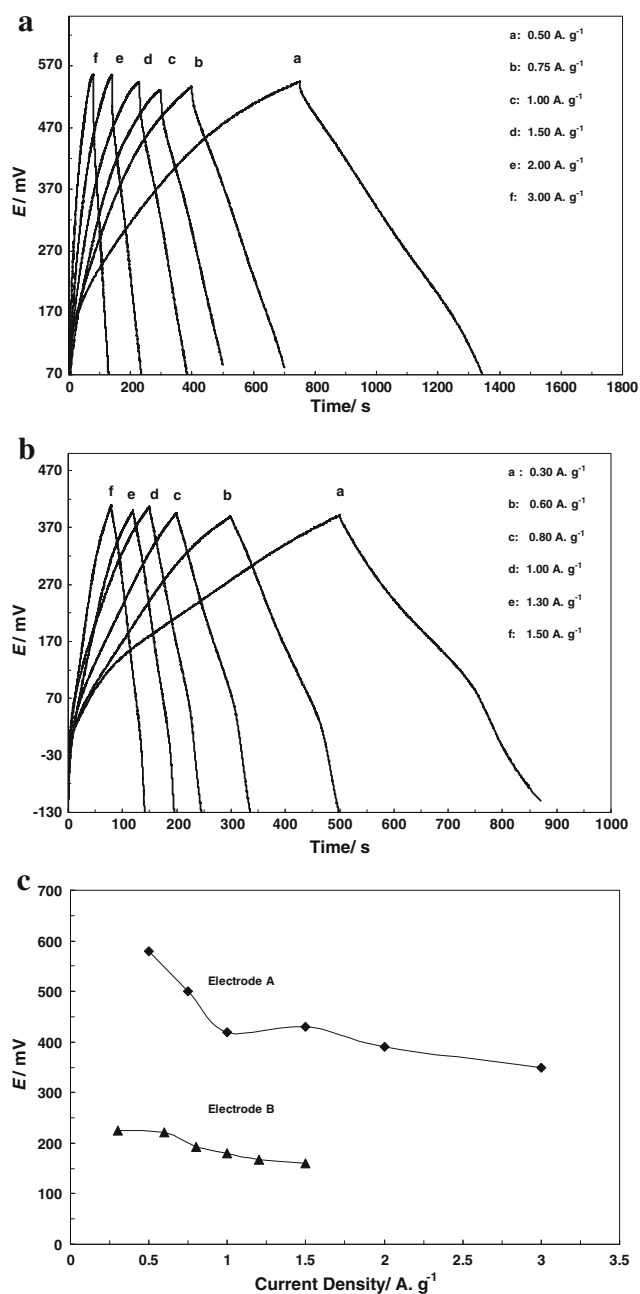
3.3 Galvanostatic charge–discharge analysis

Figure 5a, b presents the galvanostatic charge–discharge curves of the electrodes A and B examined in 1.0 M NaOH electrolyte at different current densities, respectively. As can be seen, the charge/discharge curves of both electrodes are linear and almost symmetric, indicating the capacitive behavior of the electrodes. Specific capacitance (C_{SP}) can be calculated according to the following equation [21].

$$C_{SP} = (I \times \Delta t)/(\Delta V \times m) \tag{4}$$

where I, Δt, ΔV and m denote the charge/discharge current, the discharge time, potential window and the active material mass, respectively.
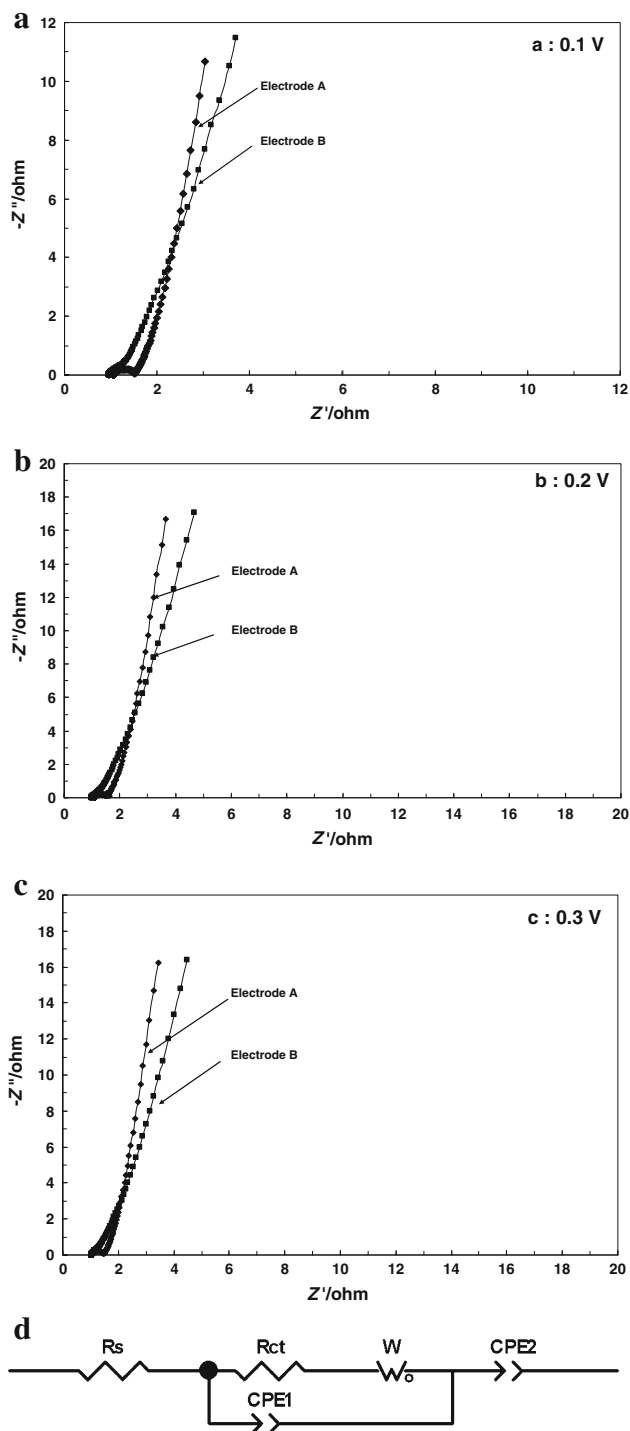
The variation of the specific capacitance with the charge/discharge current density is shown in Fig. 5c. The decrease in specific capacitance with increasing current is due to the fact that only the outer layers of Co_3O_4 can contribute to charge–discharge processes at higher current densities. At a current density of 3 A g^{-1}, the specific capacitance of the electrode A is still as high as 350 F g^{-1}, which is about 61 % of the specific capacitance at a current density of 0.5 A g^{-1}(570 F g^{-1}). In case of electrode B, the respective fall is about 71 % when current density changes from 0.3 to 1.5 A g^{-1}. Also, the specific capacitances obtained by the charge–discharge method are close to the values derived from CV studies.

Fig. 5 Galvanostatic charge/discharge cycling curves of the electrode A (**a**) and electrode B (**b**) at different current densities in 1.0 M NaOH electrolyte, variation of the specific capacitance at different current densities in 1.0 M NaOH electrolyte (**c**)

3.4 Impedance spectra of the Co_3O_4/TiO_2 nanotubes/Ti electrodes

Electrochemical impedance spectroscopy (EIS) was used to study the electrochemical behavior of the electrodes, and typical Nyquist plots are presented in Fig. 6a–c. The EIS spectra of the electrodes A and B at different applied potentials (0.1, 0.2, 0.3 V vs. Ag/AgCl) in the range of

Fig. 6 Impedance Nyquist plots of the electrode A and B at different applied voltages [0.1 V (**a**), 0.2 V (**b**), 0.3 V (**c**) vs. Ag/AgCl] and equivalent circuit for the simulation of the EIS spectra of fabricated electrodes (**d**)

Table 2 Fitting values for the equivalent circuit elements by the simulation of impedance spectra in Fig. 6d

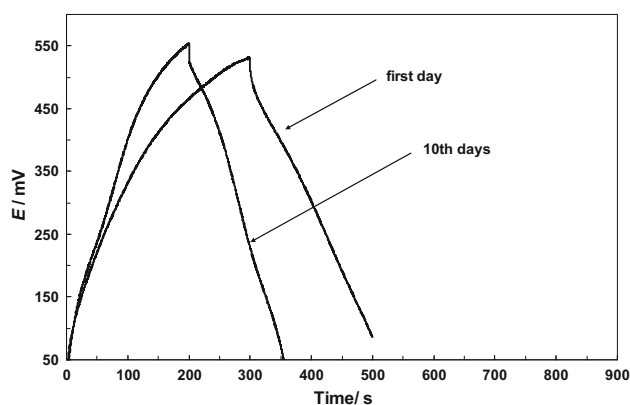| Sample	Element	E (V)		
		0.1	0.2	0.3
Electrode A	R_s (Ω)	1.06	1.09	1.04
	R_{ct} (Ω)	0.43	0.43	0.41
	W (Ω s$^{-1/2}$)	1.97	1.77	1.28
	CPE$_1$ (Ω^{-1} s)	0.0052	0.0076	0.0046
	n_1	0.92	0.87	0.94
	CPE$_2$ (Ω^{-1} s)	1.82	1.08	1.11
	n_2	0.91	0.92	0.92
Electrode B	R_s (Ω)	0.95	1.00	1.03
	R_{ct} (Ω)	0.38	0.27	0.26
	W (Ω S$^{-1/2}$)	3.6	3.7	4.0
	CPE$_1$ (Ω^{-1} s)	0.065	0.06	0.08
	n_1	0.85	0.88	0.89
	CPE$_2$ (Ω^{-1} s)	0.18	0.17	0.20
	n_2	0.87	0.86	0.88

an almost vertical line in the low-frequency end of the spectrum. In the intermediate frequencies, a line with a slope of unity which is indicative of diffusive resistance toward OH$^-$ ion transport within the Co_3O_4 electrode pores and surface layers of the electrode is observed. The diameter of the semicircle roughly represents the charge transfer resistance (R_{ct}) in Co_3O_4 film, and the almost vertical line represents the pseudocapacitive behavior of the system [22].

The parameters of the equivalent circuit are reported in Table 2. The mean error of modulus is <1 %, implying that the parameter values obtained from EIS fitting to the proposed circuits are highly reliable. The equivalent circuit parameters represent resistance of the electrolyte and the intrinsic resistance of the active material (R_s), the Warburg impedance (W) corresponds to the diffusion of OH$^-$ ions, and constant phase element (CPE$_1$) is actually the double-layer characteristic and is in parallel with a charge transfer resistance (R_{ct}) and the faradaic pseudocapacitance (CPE$_2$) of Co_3O_4 films. CPE is defined by [23]:

$$Z_{CPE} = [Q(j\omega)^n]^{-1} \tag{5}$$

where Q and n are frequency-independent constants and ω being the angular frequency of the measuring signal. The constant value of Q is related to the apparent capacitance and is directly proportional to the active area. The exponent n is a correction factor that can somehow be related to the roughness of electrode with values ranging between 0 and 1. $n = 1$ denotes that CPE element is an ideal capacitor, while $n = 0$ and 0.5 denote a resistance and Warburg behavior, respectively. In general, the appearance of a CPE may arise from: (1) a distribution of the relaxation times as

100 kHz to 10 mHz in 1.0 M NaOH are shown and the experimental results are fitted to the equivalent circuit presented in Fig. 6d. The Nyquist plot consists of a squashed semicircle in the high-frequency region terminating to

Fig. 7 Charge/discharge curves for the electrode A in 1.0 M NaOH electrolyte at a current density of 1.00 A g^{-1} for the first and 10th dyes

a result of inhomogeneities existing at the electrode/electrolyte interface; (2) porosity and (3) dynamic disorder associated with diffusion [24].

As seen from Table 2, the value of CPE$_1$ is much less than that of CPE$_2$, remains virtually the same in the both electrodes and seems to be a double-layer capacitance accompanying charge transfer processes at the interface. The result indicates that the observed large capacitance of electrodes is the pseudocapacitance produced by a fast reversible faradaic reaction, Eqs. (1, 2), which takes place at the Co$_3$O$_4$/solution interface. The value of CPE$_2$ for the electrode A is higher and can be attributed to the higher surface area and porosity of this electrode.

3.5 Stability of the Co$_3$O$_4$/TiO$_2$ nanotubes/Ti electrodes

In order to evaluate the stability of the electrode A, the specific capacitance in 1.0 M NaOH electrolyte at a constant current of 1 A g^{-1} was measured in a period of 10 days. Figure 7 shows charge/discharge curves of the first cycle and a similar cycle of the 10 days of sample being used in various electrochemical studies. A partial decrease in specific capacitance from 430 to 345 F g^{-1} has been observed showing 80 % perseverance of capacity. Data presented in Fig. 7 indicate that the electrode retains its activity over extended period of time and used in variable experiments and numerous cycles of charge/discharge.

4 Conclusion

Co$_3$O$_4$/TiO$_2$ nanotubes/Ti modified electrodes were prepared by the electroplating of Zn–Co onto TiO$_2$ nanotubes followed by dealloying of Zn–Co/TiO$_2$NTs in a concentrated

alkaline solution. The Co$_3$O$_4$/TiO$_2$ nanotubes/Ti electrode possessed extra nanoporous/cracked structures that can promote the transport of reactive species within the electrode that is beneficial to supercapacitor applications. A high specific capacitance of 430 F g^{-1} in 1.0 M NaOH electrolyte at a constant current density of 1 A g^{-1} was obtained. The performance and stability of the electrode were tested by constant current charge–discharge cycling over periods of days. The specific capacitance maintained 80 % of initial value upon 10 days of prolonged studies.

References

1. F. Markoulidis, C. Lei, C. Lekakou, Appl. Phys. A doi:10.1007/s00339-012-7471-8
2. S.G. Kandalkar, J.L. Gunjakar, C.D. Lokhande, Appl. Surf. Sci. **254**, 5540 (2008)
3. T. Cottineau, M. Toupin, T. Delahaye, T. Brousse, D. Belanger, Appl. Phys. A **82**, 599 (2006)
4. Y. Gao, S. Chen, D. Cao, G. Wang, J. Yin, J. Power Sources **195**, 1757 (2010)
5. W.C. Li, G.Z. Nong, A.H. Lu, H.Q. Hu, J. Porous Mater. **18**, 23 (2011)
6. W. Kim, M.Y. Kang, J.B. Joo, N.D. Kim, I.K. Song, P. Kim, J.R. Yoon, J. Yi, J. Power Sources **195**, 2125 (2010)
7. F. Gobal, M. Faraji, J. Electroanal. Chem. **691**, 51 (2013)
8. Y. Xie, D. Fu, Mater. Chem. Phys. **122**, 23 (2010)
9. Y. Wang, H. Wang, X. Wang, Electrochim. Acta **92**, 298 (2013)
10. R. Tummala, R.K. Guduru, P.S. Mohanty, J. Power Sources **209**, 44 (2012)
11. R.P. Antony, T. Mathews, S. Dash, A.K. Tyagi, B. Raj, Mater. Chem. Phys. **132**, 957 (2012)
12. I. Herraiz-Cardona, E. Ortega, V. Pérez-Herranz, Electrochim. Acta **56**, 1308 (2011)
13. D.K. Pawar, J.S. Shaikh, B.S. Pawar, S.M. Pawar, P.S. Patil, S.S. Kolekar, J. Porous Mater. **19**, 649 (2012)
14. Y. Li, K. Huang, S. Liu, Z. Yao, S. Zhuang, J. Solid State Electrochem. **15**, 587 (2011)
15. Y.Q. Zhang, X.H. Xia, J. Kang, J.P. Tu, Chin. Sci. Bull. **57**, 32 (2012)
16. D. Kalpana, K.S. Omkumar, S. Suresh Kumar, N.G. Renganathan, Electrochim. Acta **52**, 1309 (2006)
17. M. Selvakumar, D. Krishna Bhat, A. Manish Aggarwal, S. PrahladhIyer, G. Sravani, Phys. B **405**, 2286 (2010)
18. N. Padmanathan, S. Selladurai, Ionics **20**, 409 (2014)
19. N. Padmanathan, S. Selladurai, Ionics **20**, 479 (2014)
20. X. Wang, S. Liu, H. Wang, F. Tu, D. Fang, Y. Li, J. Solid State Electrochem. **16**, 3593 (2012)
21. K.S. Kim, S.J. Park, J. Solid State Electrochem. **16**, 2751 (2012)
22. Y.F. Li, Y.Z. Liu, Y.G. Yang, M.Z. Wang, Y.F. Wen, Appl. Phys. A **108**, 701 (2012)
23. C. Xia, Y. Xie, Y. Wang, W. Wang, H. Du, F. Tian, J. Appl. Electrochem. **43**, 1225 (2013)
24. T.C. Girija, M.V. Sangaranarayanan, J. Power Sources **156**, 705 (2006)